Metallization of aluminum hydride AlH$_3$ at high multiple-shock pressures

A. M. Molodets,[1],[*] D. V. Shakhray,[1] A. G. Khrapak,[2] and V. E. Fortov[2]

[1]*Institute of Problems of Chemical Physics, RAS, 142432 Chernogolovka, Russia*
[2]*Joint Institute for High Temperatures, RAS, 125412 Moscow, Russia*

A study of electrophysical and thermodynamic properties of alane AlH$_3$ under multishock compression has been carried out. The increase in specific electroconductivity of alane at shock compression up to pressure 100 GPa has been measured. High pressures and temperatures were obtained with an explosive device, which accelerates the stainless impactor up to 3 km/s. A strong shock wave is generated on impact with a holder containing alane. The impact shock is split into a shock wave reverberating in alane between two stiff metal anvils. This compression loads the alane sample by a multishock manner up to pressure 80–90 GPa, heats alane to the temperature of about 1500–2000 K, and lasts 1 μs. The conductivity of shocked alane increases in the range up to 60–75 GPa and is about 30 $(\Omega \, \text{cm})^{-1}$. In this region the semiconductor regime is true for shocked alane. The conductivity of alane achieves approximately 500 $(\Omega \, \text{cm})^{-1}$ at 80–90 GPa. In this region, conductivity is interpreted in frames of the conception of the "dielectric catastrophe," taking into consideration significant differences between the electronic states of isolated molecule AlH$_3$ and condensed alane.

I. INTRODUCTION

Aluminum hydride α-AlH$_3$ (alane) is a solid with very large hydrogen content of 10.1 wt%. Aluminum hydride is a promising additive to rocket fuels and high explosives, and so need for knowledge of its properties under high pressures and temperature appears. Aluminum hydride has been intensely studied as one of the most promising materials for hydrogen storage. The large hydrogen content of AlH$_3$ leads to other interesting properties. It was noticed[1] that "light" hydrides (such as CH$_4$, SiH$_4$, AlH$_3$, or MgH$_2$) might also be high-T_c superconductors. Recently possible metallization of alane at high pressure along the room-temperature isotherm up to 100 GPa has been investigated theoretically[2] and experimentally.[3] The results obtained are sufficiently encouraging to prompt studies of a wider range of temperatures. In this paper, the electrical conductivity of AlH$_3$ has been studied under multishock compression up to 100 GPa and temperature up to 2000 K.

II. SAMPLES, SHOCK LOADING, AND MEASURING CELL

The starting material was powder of α-AlH$_3$ with a grain size of 30 μm and a purity of 99.8 wt % produced by a reaction of LiAlH$_4$ with AlCl$_3$ in ether solution at room temperature.[4] This powder was earlier characterized by inelastic neutron scattering[5] and x-ray diffraction and calorimetry.[6] The samples for the shock experiments were thin disks (10 mm in diameter and 0.5 mm thick) made by pressing the powder at room temperature.

After compacting the surfaces of the sample was flat that provided better electrical contact with copper measuring electrodes. The initial density of the disk samples was 1.23−1.41 g/cm^3. Disk sample 1 (see Fig. 1) was inserted into the Teflon film 2.

The sample was located on the axis of the experiment. The manganin shock pressure gauge 3 was located at 5 mm

from the sample. Two additional Teflon film 4's were on and under the Teflon film 2 with the sample and the gauge. The resulted "sandwich" 1–4 was pressed between two copper plates.

The shock wave loading was realized by the impact of steel plate-projectile (see Fig. 1) with diameter 90 mm. The projectile was accelerated by the explosion products up to the velocity $W=2.6(1)−3.15(9)$ km/s, the planar region of the projectile at impact was 60 mm and the variation in impact time over the projectile was less than 0.1 μs.[7] Reference 7 contains comprehensive data on the launch setup. The stainless projectile generated a shock wave in the first copper plate. Then the Teflon sandwich together with the sample and the manganin gauge were subjected to the step increasing of the shock pressure as a result of reverberations of the shock waves between tungsten anvils and cooper plates. The shock pressure was registered by the manganin gauge. The pressure reached about 100 GPa in our experiments.

The initial electric resistance of the samples was greater than 10^6 Ω. The electric resistance of the AlH$_3$ sample under
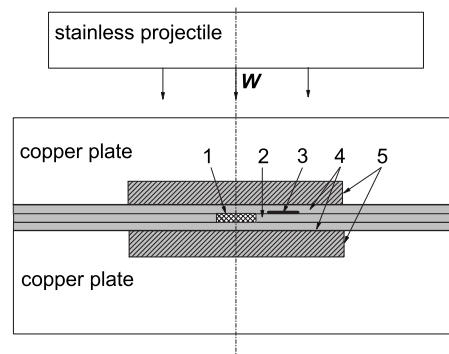

FIG. 1. The scheme of the cell for electric measurements under step shock wave loading. 1 is the alane sample, 2 is the Teflon film with thickness 0.5 mm, 3 is the manganin gauge, 4 is the Teflon films with thickness 1 mm, and 5 is the tungsten disks with thickness 1.5 mm and diameter 24 mm.
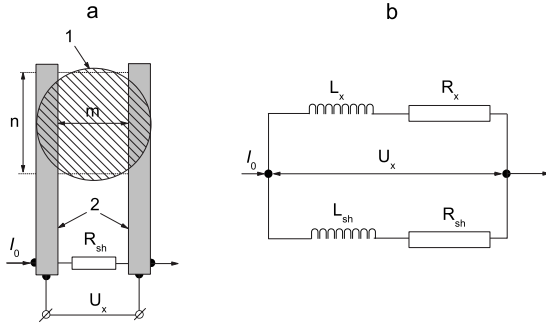
FIG. 2. (a) Measuring cell and (b) equivalent circuit of sample conductivity gauge. (a) 1 is disk sample of thickness $h_0 = 0.5$ mm and effective sizes $m = 3-5$ mm and $n = 6-8$ mm, 2 is copper current leads, R_{sh} is the shunting resistor; (b) R_x is the sample resistance, L_x is the inductance of the sample, R_{sh} is the shunting resistor, L_{sh} is the inductance of the shunt resistor, and U_x is the copper electrode voltage.

FIG. 3. (Color online) The experimental profiles (time dependencies) of the AlH$_3$ sample electric conductivity $S_i(t)$ and pressure $P(t)$ under multishock wave loading up to ≈ 70 GPa. 1 is an experimental profile $P(t)$ in the environment (the Teflon), 2 is a calculated profile $P(t)$ in α-AlH$_3$ sample, 3 is an experimental profile $S_i(t)$ for α-AlH$_3$, and 4 is an experimental profile $S_i(t)$ for Teflon.

step shock effect was measured out simultaneously with the registration of the pressure at shock compression. The measuring cell is shown in [Fig. 2(a)] schematically. The measuring electrodes were made from copper foil with the 3 mm wide and the thickness of 0.02 mm. That is to say the thickness of copper electrodes was much smaller the sample thickness (0.5 mm). This thickness ratio suggests that three-dimensional (3D) effect from the copper electrode, etc. is small and can be neglected. The direct current $I_0 \approx 10$ A was passed along the sample and the shunt resistor $R_{sh} \cong 2.5$ Ω before and during the shock loading of the sample. The equivalent circuit of the measuring cell was submitted in Fig. 2(b). The voltage $U_x = U_x(t)$ depending on time t was measured on the copper electrodes. The U_x measurement was done by oscilloscope Tektronix TDS-744A. The electric resistance of the sample in the scheme Fig. 2(b) was calculated according to[8]

$$U_x = I_0 R_{sh} \left\{ \frac{R_x}{R_{sh} + R_x} + \left(\frac{R_{sh}}{R_{sh} + R_x} - \frac{L_x}{L_x + L_{sh}} \right) \exp\left(-\frac{R_{sh} + R_x}{L_{sh} + L_x} t \right) \right\}, \quad (1)$$

where the nil moment of the time $t = 0$ corresponds to the moment of shock wave arrival at the sample. The transition time τ in this scheme is

$$\tau \approx 3 \frac{L_x + L_{sh}}{R_x + R_{sh}}. \quad (2)$$

In this work the total inductance $L_x + L_{sh}$ was equal about 10^{-8} H that under $R_{sh} \cong 2.5$ Ω gave the τ order of magnitude 0.01 μs. So, at the write time about $0.1-1$ μs limiting form (1) was used, corresponding to an infinitely small term in braces of Eq. (1). In this approach the sample resistance R_x was calculated by measured value U_x as

$$R_x = \frac{U_x R_{sh}}{U_x + I_0 R_{sh}}. \quad (3)$$

In the arrangement shown in Fig. 1, we carried out two series of experiments with different impactor velocity W. In the first series, tungsten disk 5 was absent and the maximum pressure of shock compression amounted to ≈ 70 GPa. The second series of experiments was carried out with tungsten disks, which led to an increase the pressure of shock compression up to ≈ 100 GPa. The best typical experimental profiles of pressure and conductivity $S_i = 1/R_x$ are shown in Figs. 3 and 4 for the maximum pressures of each series.

The magnitude of the electrical conductivity of the Teflon at the experimental conditions was estimated in the specific shot. The measuring cell 1a (see Fig. 2) with the Teflon film 2 (see Fig. 1) without the sample was used. The experimental profile $S_i(t)$ for Teflon shown in Fig. 3. From this figure we notice that the magnitude of the electrical conductivity of the Teflon is negligible.

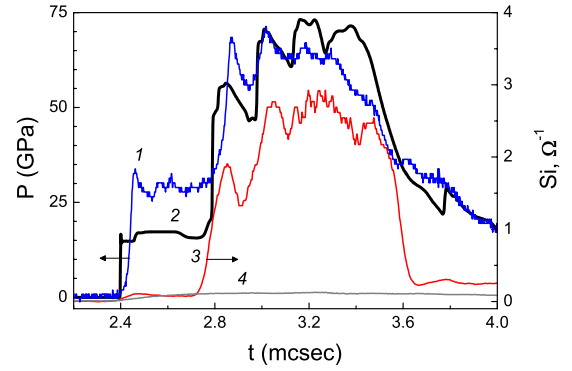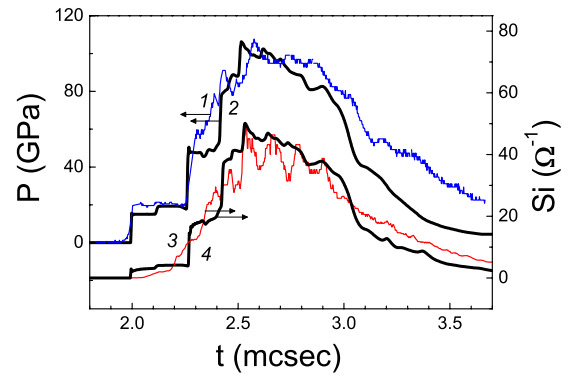The specific conductivity $\sigma = \sigma(t)$ was calculated as

FIG. 4. (Color online) The experimental profiles (time dependencies) of the AlH$_3$ sample electric conductivity $S_i(t)$ and pressure $P(t)$ under multishock wave loading up to ≈ 100 GPa. 1 is an experimental profile $P(t)$, 2 is a calculated profile $P(t)$ in AlH$_3$-III sample, 3 is an experimental profile $S_i(t)$, and 4 is a calculated profile $S_i(t)$.

TABLE I. The parameters for equation of state [Eq. (5)] of α-AlH$_3$, AlH$_3$-III, and Al

Solid	v_s (cm^3/mol)	S_1 (GPa)	S_2 (GPa)	S_3 (kJ/g)	V_0 (cm^3/mol)	γ_{0s}	γ_0
α-AlH$_3$	57.65	−41.64	858.12	−840.45	20.14	1.74	0.76
AlH$_3$-III	34.10	−146.58	3046.12	−1739.24	15.74	2.38	2.38
Al	25.73	−110.81	2293.62	−1106.77	10.0	1.94	1.94

$$\sigma = C\frac{V_0}{V}S_i, \qquad (4)$$

where V_0 and V are the initial and current specific volumes, C is a geometry-dependent parameter called the cell constant. The parameter C was calculated as $C=m/nh_0$, where m, n, and h_0 were the geometries of the sample [see Fig. 2(a)].

III. THERMODYNAMIC PARAMETERS AND EQUATION OF STATE OF ALANE

The numerical calculation of the shock wave interaction and the release wave in the cell was carried out to obtain details of the pressure-temperature dependence of the conductivity of alane under step shock loading. The one-dimensional flat flow corresponding to experiment (Fig. 1) was simulated. The numerical calculation was carried out using the modified "individual particle-in-cell" method[9] at a flat unidimensional approach. The Mie-Gruneisen equations of state for metals were used in the semiempirical form.[10,11]

This equation of state for alane was constructed in the semiempirical form[10] as well,

$$P - P_s = \frac{\gamma}{V}(E - E_s), \qquad (5)$$

where P is the pressure, E is the energy, and V is the volume; $P_s=P_s(V)$ and $E_s=E_s(V)$ are correspondingly volume dependencies of pressure and energy along an isotherm $T=T_0$ =const; $\gamma=\gamma(V)$ is the volume dependence of the Gruneisen factor.

The formulas for the lattice components of E_s and P_s were taken from Ref. 10. The energy E_s was determined by the following expressions.

$$E_s = -v_s(S_1 H_x + S_2 x) + S_3 + T_0[S(x,T_0) - S(x_0,T_0)], \qquad (6)$$

$$S = 3R\left(\frac{4}{3} - \ln\frac{\Theta(x)}{T}\right), \qquad (7)$$

$$\Theta = \Theta_0\left(\frac{1-x}{1-x_0}\right)^2\left(\frac{x_0}{x}\right)^{2/3}, \qquad (8)$$

$$H_x = 9\left(\frac{1}{10}x^{-2/3} + 2x^{1/3} + \frac{3}{2}x^{4/3} - \frac{1}{7}x^{7/3} + \frac{1}{70}x^{10/3}\right), \qquad (9)$$

$$x = \frac{V}{v_s}, \quad x_0 = \frac{V_0}{v_s}, \qquad (10)$$

where S_1, S_2, and v_s are the fitting parameters, S is the entropy, Θ is the characteristic temperature, $V_0=V(P_0,T_0)$, P_0 =1 atm, $T_0=298$ K, R is a specific gas constant, and S_3 is an integration constant defined from initial conditions. The constant S_3 is defined so that the value $E_s(x)$ in the minimum point $x=x_{min}$ was zero $E_s(x_{min})=0$.

The pressure P_s was determined with the help of the second law of the thermodynamics $P_s=-\frac{dE_s}{dV}+T_0\frac{dS}{dV}$ and volume derivatives [Eqs. (6) and (7)];

$$P_s = S_1 F_x + S_2, \qquad (11)$$

$$F_x = \frac{dH_x}{dx} = 3\left(-\frac{1}{5}x^{-5/3} + 2x^{-2/3} + 6x^{1/3} - x^{4/3} + \frac{1}{7}x^{7/3}\right). \qquad (12)$$

The expression for $\gamma=\gamma(V)$, which is defined by means of the first and second derivatives from Eq. (11) with the help of Slater's formula, was used in Ref. 10,

$$\gamma = -\frac{2}{3} - \frac{V}{2}\frac{d^2 P_s/dV^2}{dP_s/dV} = \frac{2}{3} + \frac{2V}{v_s - V}, \qquad (13)$$

but for α-AlH$_3$ Eq. (13) was replaced on

$$\gamma = \frac{2}{3} + \frac{2V}{v_0 - V}, \qquad (14)$$

where v_0 was calculated as

$$v_0 = V_0\left(1 + \frac{2}{\gamma_0 - 2/3}\right), \qquad (15)$$

with $\gamma_0=\beta K_0 V_0/C_V=0.76$ as the thermal Gruneisen parameter for α-AlH$_3$ from Ref. 6.

The fitting parameters S$_1$, S$_2$, and v_s were determined with help of the least-squares method from condition of the best description of the experimental high-pressure isotherms[3] by Eq. (11). The complete set of parameters for equation of state for α-AlH$_3$ and high-pressure phase AlH$_3$-III are listed in Table I. The parameters of the Al equation of state are listed in Table I. They are determined in Ref. 12 under experimental high-pressure isotherm.[13] The corresponding plots of Eq. (11) are shown in Fig. 5.

The calculation of shock pressure P_h and shock energy E_h for monolithic material are carried as in Ref. 10 by using known shock physics formulas with the equations of state [Eq. (5)] with parameters from Table I;
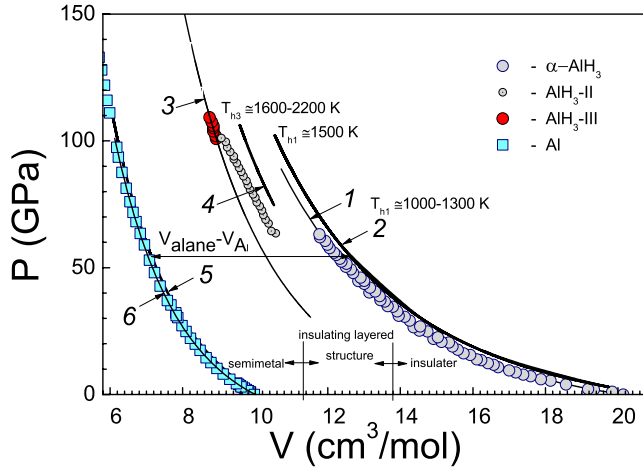
FIG. 5. (Color online) Pressure *P*-volume *V* relationship at an isothermal and multishock compression of alane and aluminum. The dotes are the experimental high pressure isotherms of α-AlH$_3$, AlH$_3$-II, and AlH$_3$-III (Ref. 3), squares are the data for Al (Ref. 13). The double arrows show the theoretical prediction of layered insulator and semimetal region (Ref. 2). 1, 3, and 6 are the plots of Eq. (11) for α-AlH$_3$, AlH$_3$-III, and Al, respectively. 2 is the phase trajectory of multishock compression of α-AlH$_3$ up to 73 GPa and 4 is the phase trajectory of multi shock compression of AlH$_3$-III in region 80–100 GPa. The numerals are temperatures in these states. 5 is the phase trajectory of multishock compression of Al in region 0–100 GPa in the same conditions.

$$P_h = \frac{P_s - \frac{\gamma}{V}[E_s - E_s(x_0, T_0)]}{1 - \frac{\gamma}{2V}(V_0 - V)}, \tag{16}$$

$$E_h = E_s(x_0, T_0) + \frac{1}{2}(P_h + P_0)(V_0 - V). \tag{17}$$

There is a wide range of initial densities, and some samples have significant porosity. One would expect a much higher temperature for a porous sample than a fully dense sample. Also, the spread of initial densities would suggest than a slightly different thermodynamic path for each sample. Therefore the calculation of shock pressure P_{hp} and energy E_{hp} for porous materials with porosity m and initial specific volume $V_{00} = mV_0$ was carried out by the somewhat different formulas of shock compression physics.

The pressure P_{hp} was calculated as

$$P_{hp} = \frac{P_h\left[1 - \frac{\gamma}{2V}(V_0 - V)\right]}{1 - \frac{\gamma}{2V}(V_{00} - V)}. \tag{18}$$

The energy E_{hp} is calculated by formula (17) where P_h is substituted for P_{hp} and V_0 is replaced by V_{00}.

The temperature T_{hp} along porous Hugoniot is found as the root of the equation

$$E_{hp} - E_s = \int_{T_0}^{T_{hp}} C_V dT, \tag{19}$$

where $C_V = C_V(T_h)$ is the temperature dependence of isochoric heat capacity. The temperature dependent $C_V = C_V(T)$ of
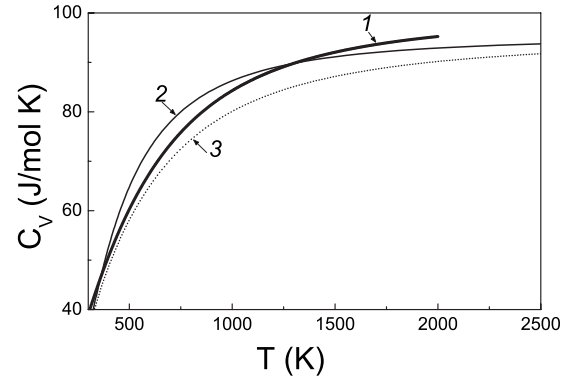

FIG. 6. The $C_V(T)$ dependences of α-AlH$_3$. 1 is the experiment at atmospheric pressure (Ref. 6), 2 is the plot of Eq. (20), and 3 is the estimation of $C_V(T)$ along the Hugoniot.

α-AlH$_3$ was taken from Ref. 6. The experimental data $C_V(T)$ (Ref. 6) (see curve 1 in Fig. 6) within the range of 300–2000 K were approximated (see curve 2 in Fig. 6) by an Einstein-type function

$$C_V = a\frac{(b/T)^2}{[\exp(b/T) - 1]^2}\exp(b/T), \tag{20}$$

where $a = 95.24$ J/(mol K) and $b = 1093$ K.

It would appear reasonable that the heat capacity to vary significantly with compression as well as temperature. This effect is estimated under the assumption that b is the volume function $b = \theta(V)$, where $\theta(V)$ is the characteristic temperature of Eq. (8) with $\theta_0 = 1093$ K. In this approach the heat capacity of alane along the Hugoniot shown in Fig. 6 by curve 3. One can distinguish between these curves no more than 8% at 1000–2500 K. In view of this estimation and taking into account that alane is non-Debye solids,[6] we used the simplest formula [Eq. (20)] with $b = $const$ = 1093$ K.

The calculations of the thermodynamic states under maximum pressure 73 GPa for α-AlH$_3$ and within the range of 80–100 GPa for AlH$_3$-III are shown in Fig. 5. The calculated pressure profiles $P(t)$ for AlH$_3$ are shown in Figs. 3 and 4. In Fig. 7 the calculation of the thermodynamic path shown in
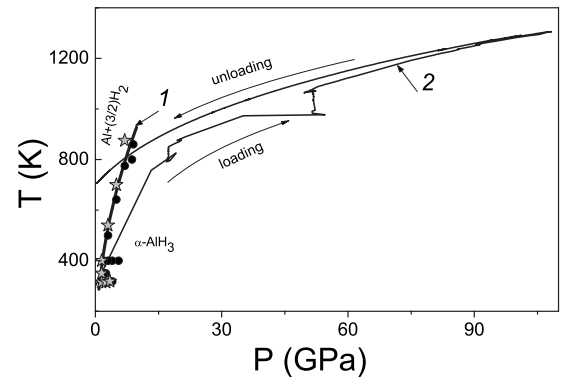

FIG. 7. *T*-*P* diagram of Al–H system. 1 is the equilibrium Al+(1.5)H$_2$=AlH$_3$ (Ref. 14), 2 is the calculated of multishock thermodynamic path, stars, and points (Ref. 14) are AlH$_3$ and Al+(1.5)H$_2$, respectively.

T-*P*-coordinates as against the static decomposition curve.[14] The thermodynamic path is placed under the decomposition curve. This suggests the lack of any decomposition alane under the multiple-shock compression.

IV. RESULTS AND DISCUSSION

A. Results at low pressures

The comparison of conductivity profiles and corresponding pressure profiles allows to draw the following conclusions. The conductivity of shocked compressed alane up to pressures 20–25 GPa is the value around ~ 0.01 Ω^{-1}. Within the range of pressures 30–75 GPa the conductivity greatly increases and reaches 2–3 Ω^{-1} (see Fig. 3). It is possible to suppose that the sharp change of sample conductivity in the range of ≈ 30 GPa is determined by the transition of insulating low-pressure α phase to an insulating layered structured, theoretically predicted for this pressure range in (Ref. 2).

Let us notice that the sample conductivity within the range of pressures 30–70 GPa has a reversible nature (see Fig. 3). It grows with the shock pressure increasing (and consequently the increasing of the shock temperature) and decreases with the reduction of these parameters in unloading. The calculations of the shock temperature T_{h1} in the range of 30–70 GPa give rather high values T_{h1} $\approx 1000-1300$ K (see Fig. 5). So it may be that the alane sample conductivity in the layered insulator range is caused by the increase in current carrier concentration under growing temperature. The argument for such a semiconductor mechanism is a possibility of the description of conductivity profiles by typical exponential ratio for temperature dependency of specific conductivity σ as

$$\sigma = \sigma_0 \exp\left(-\frac{E_g(V)}{2kT}\right). \tag{21}$$

Really, according to Ref. 2 the minimum values of band gap E_{g0} for different alane structures within the range up to 80 GPa are $E_{g0} = 0.36-0.90$ eV. Thereupon the value of band gap might be equal $E_{g0} = 0.6$ eV. At the same time in accordance with Ref. 2 it is supposed that the band gap decreases with pressure.

The decreasing factor of E_{g0} under pressure growth in Eq. (21) may be taken into account in the ratio of the volume V to volume V_{0i}, where V_{0i} is the volume of transition insulator into layered insulator at 34 GPa (Ref. 2) equal $V_{0i} = 13.78$ cm³/mol. In other words, we can expect that the band gap E_g in Eq. (21) depends on the volume as $E_g = E_g(V) = E_{g0}V/V_{0i}$. Equation (21) with these parameters, being a built-in gas dynamic code allows us to calculate the resistance of a shock compressing sample. This calculation executed under specially selected constant σ_0 is shown by line 2 in Fig. 8. Evidently it is possible to interpret the experimental conductivity profile 1 of alane in the field of 30–75 GPa in details. The meaning of constant σ_0 has herewith the value $\sigma_0 = 148$ $(\Omega \text{ cm})^{-1}$.

We note that the nature of conductivities under multi-shock compression AlH₃ has a close analogy with conduc-
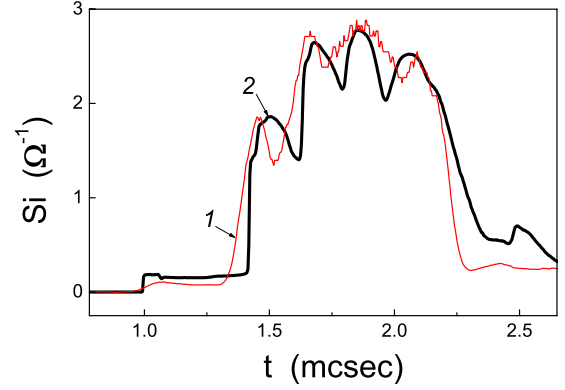

FIG. 8. (Color online) Simulation of conductivity of shocked alane in the semiconductor regime. 1 is the experimental oscillogram and 2 is the model profile of the sample conductivity available by using Eq. (21) in layered insulator region.

tivity of shocked hydrogen from Ref. 15. To show this, we present the data of conductivities in coordinates $\sigma - V_H$, where V_H is a partial volume of hydrogen. For shocked hydrogen $V_H = V_{H2}/2N_a$, where V_{H2} is a molar volume of molecular hydrogen from Ref. 15, N_a is the Avogadro number.

In the case of the room-temperature isotherm one commonly estimates the partial hydrogen volume V_H in the hydride from subtraction of the atomic volume of pure aluminum measured at the same pressure (see Ref. 3). Let us use this technique for alane phase paths (lines 2 and 4) and for aluminum (line 6) (see Fig. 5). In this approach the partial volume of the hydrogen in shocked compressed AlH₃ will be equal $V_H = (V_{alane} - V_{Al})/3N_a$ where V_{alane} is an alane molar volume and V_{Al} is an aluminum molar volume.

The conductivity data in the coordinate σ-V_H are shown in Fig. 9. The value σ for AlH₃ is close to σ for H at $V_H = 2.65-2.75$ Å³/atom.

Moreover as stated above the conductivity of the alane has a semiconductor nature similar to the conductivity of shocked hydrogen in (Ref. 15). Note that even pre-exponential factor σ_0 is the same in both cases and equal to 148 $(\Omega \text{ cm})^{-1}$.
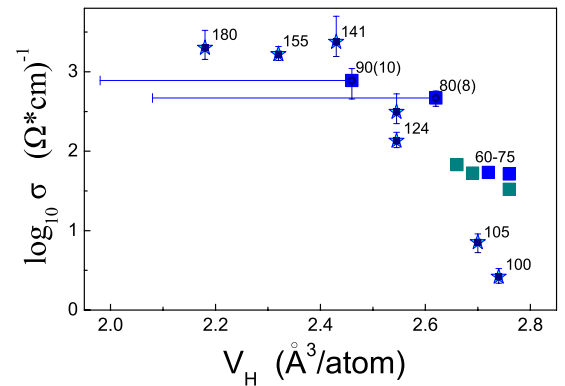

FIG. 9. (Color online) Conductivity of alane and fluid hydrogen as a function of partial hydrogen volume V_H. Stars are the data (Ref. 15), squares are the data of the present work. Volume error is the uncertainty in the calculations (see text). Numerals are specified the magnitudes of maximum shock pressures in GPa. The accuracy of the pressure is indicated in the brackets.

B. Results at high pressures

We shall notice that the area 80–100 GPa in Fig. 5 corresponding to $V_H = 2.6–2.4$ Å^3/atom in Fig. 9 is the area of several high-pressure phases. They are an semimetal area according to Ref. 2, as well as a polymorphic transitions α-AlH$_3 \leftrightarrow$ AlH$_3$-II and AlH$_3$-II $\leftrightarrow$ AlH$_3$-III according to Ref. 3, and also probable melting or even decompositions of alane in a shock wave. It is not clear from the experimental data that these irreversible processes do not occur. The absence of the phase diagram and thermodynamic properties of the high-pressure phases AlH$_3$-II and AlH$_3$-III do not allow really to calculate the shock compression parameters in this area. Thus under such conditions, it would be unclear whether the current equation of state analysis would be valid. But we estimated the thermodynamic alane condition limits in carried out experiments as follows.

The minimum values of the temperatures and densities correspond to the calculations carried out the assumption that no phase transitions in alane take place and the substance follows the equation of state α-AlH$_3$. In this case the volume decreases along curve 2 and maximum temperatures reach the values $T_{h1} \approx 1500$ K (see Fig. 5). In the other limit case it is supposed that in strong shock waves alane falls into the area of phase AlH$_3$-III, the equation of state which is presented in Table I. Here the volume decreases along curve 4 and maximum temperatures reach values $T_{h3} \approx 1600–2200$ K (see Fig. 5).

In accordance with these estimations the partial volumes uncertainty V_H is marked off at pressures 80–90 GPa in Fig. 9. The points correspond to the compression of alane along curve 2 in Fig. 5. Inaccuracy toward a small volume corresponds to the compression of alane along curve 4 in Fig. 5.

Within the framework of these approach it is possible to say that the quantitative analogy between conductivity of the hydrogen and alane is seen and under higher pressures. So in Fig. 5 at $V_H = 2.45–2.60$ Å^3/atom the strong growth of alane conductivity reaching the hydrogen conductivity values is observed. At the same time it should be noted that in this region the conductivity mechanism of alane and hydrogen is different. In Ref. 15 the conductivity of hydrogen gains the metallic nature but in the case of shocked alane, most likely the semiconductor mechanism of conductivities remains. The conductivity profile (see Fig. 4) in the high-pressure region is the evidence of such suggestions, i.e., a conductivity under maximum pressure values keeps track the profile of the pressure, and signifies a temperature profile. The calculation of sample conductivity profile at 100 GPa under Eq. (21) with a suitable C parameter is shown in Fig. 4. The simulated profile retraces the same experimental profile. This suggests the conductivity increases with the increase in the temperature that is typical for a semiconductor mechanism of conductivity.

C. Dielectric catastrophe and insulator-metal transition

The experimental regularities of the alane conductivity behavior at high pressures and temperatures of the shock compression can be interpreted in frames of so called "dielectric catastrophe" conception.[16–19] According to Herzfeld-Goldhammer criterion, the dielectric-conductor transition takes place when permittivity of a matter ϵ begins to rise sharply and amounts to values exceeded unity significantly. The dependence of the permittivity on the molecule density n of a majority of dielectrics independently on their aggregate state is described with a good accuracy by the Clausius-Mossotti equation

$$\epsilon = \frac{1 + 2b}{1 - b}, \quad b = \frac{4\pi}{3}\alpha n, \qquad (22)$$

where $b < 1$ is the refractivity and α is the polarizability. The Herzfeld criterion for the onset of a polarization divergence cannot compete with more consistent theoretical methods of calculation for locating transition between insulating and metallic phases, but it is quite reasonable for first estimations.[1,20] In the case of AlH$_3$ it is necessary to take into account that in accordance with the Pauling conception of the electronegativity (electronegativities of Al and H are equal to 1.61 and 2.20, correspondingly) in the molecule AlH$_3$ outer electrons of the Al are transferred to the H atoms[2] and the permittivity is determined by the polarizability of the ions Al^{3+} and H$^-$;

$$\alpha_{\text{AlH}_3} \cong \alpha_{\text{Al}^{3+}} + 3\alpha_{\text{H}^-}. \qquad (23)$$

Since the ionization potential of the ion Al^{3+} is high ($I_{\text{Al}^{3+}} = 120$ eV), then its polarizability is small and can be neglected in Eq. (23). In view of estimation of the α_{H^-} value it is necessary to take into consideration the fact that the Bohr radius of the outer electron of the ion H$^-$ in the vacuum ($r_i = 3.1$ Å) exceeds significantly the distance between hydrogen atoms in the crystal, as well the size of the elementary crystal cell. The exchange interaction between electrons of the neighboring ions H$^-$ results in significant decrease in the region occupied by each electron and, as consequence, in decrease in the ion polarizability. This was clearly demonstrated in Ref. 21 where the dependence of the α_{H^-} on the confining force, adjusted in the form of the parabolic potential, was determined. For an estimation of the α_{H^-} we use semiempirical method, mainly similar to the method of the estimation of the polarizability of oxides and fluorides, proposed in Ref. 22. As a basis we take values of the permittivity of a number of metal hydrides calculated in Ref. 23 and shown in Table II. Let us suggest that the Clausius-Mossotti equation is valid for all these hydrides and a contribution of positive ions in the polarizability can be neglected. Using Eq. (22) and calculated values of ϵ one can get an estimation of α_{H^-}. Obtained values of α_{H^-} are also listed in Table II.

Results obtained by investigation of properties of the magnesium hydride at high pressures[24] can be considered as additional argument in favor of the proposed estimation of the polarizability. Both the experimental and theoretical charge-density maps clearly demonstrated ionic character of all MgH$_2$ polymorph modifications and gave possibility to estimate radii of the ions Mg^{2+} (0.69 Å) and H$^-$ (1.26 Å). Knowing of the ion radius allows one to estimate the ion polarizability ($\alpha_i = R_i^3$). This gives, for the polarizability of

TABLE II. Permittivity ϵ, density ρ at normal conditions, atomic hydrogen concentration n, refractivity b, and polarizability of atomic hydrogen negative ion in condensed metal hydrides α_{H^-}

Material	ϵ	ρ (g cm^{-3})	n (cm^{-3})	b	α_{H^-} (a.u.)
LiH	4.28	0.82	6.2×10^{22}	0.50	12.4
NaH	3.03	1.40	3.5×10^{22}	0.40	18.4
MgH$_2$	3.90	1.45	3.3×10^{22}	0.49	11.9
AlH$_3$	4.43	1.49	3.0×10^{22}	0.53	9.6

the ion H$^-$ in the condensed magnesium hydride, the value 13.4 a.u., which is in a reasonable agreement with result of our estimation (11.9 a.u.).

Thus, for rough estimation the polarizability of the alane molecule in the crystal state one can take a value equal to 9.6 a.u. It exceeds the polarizability of the hydrogen atom in vacuum approximately in two times. With such polarizability the dielectric catastrophe has to begin at $n=5.6 \times 10^{22}$ cm^{-3} or $\rho=2.8$ g cm^{-3}, what is in agreement with our results and with experiments of Goncharenko et al.[3] Proposed model can be used for estimations of the transition density to the conductive state for other metal hydrides such as MgH$_2$, NaH, and LiH.

Let us discuss possible mechanism of the alane conductivity. At normal conditions valence electrons of aluminum are trapped by hydrogen atoms forming negative ions H$^-$. The resulting electron energy band is fully occupied and condensed alane is a good insulator. The energy of the electron transition from H$^-$ to Al^{3+} is equal about 3.5 eV.[2,23] It corresponds to the band gap. By increasing the temperature a part of the electrons turns to aluminum, neutral atoms of hydrogen appear in the system, and migration of electrons from H$^-$ to H becomes possible. Such mechanism of the electron transfer can explain the semiconductor character of the alane conductivity observed in experiment. By increasing the density the permittivity also increases. This results in the decrease in electron binding energy in ion H$^-$ and, consequently, in the decrease in band gap. At high enough density the band gap disappears and the conductivity gains the metallic character. The density when the permittivity becomes infinite can be obviously used as the upper estimate of the

transition density between insulating and metallic phases.

V. CONCLUSIONS

A study of electrophysical and thermodynamic properties of alane AlH$_3$ under high multishock compression has been carried out. The equations of state α-AlH$_3$ as well as for high-pressure phase AlH$_3$-III were constructed. The pressure-temperature states of alane were calculated at multishock compression. The increase in conductivity of alane at multishock compression up to pressure 80–90 GPa, temperature about 1500–2000 K and within 1 μs has been measured. The conductivity of shocked alane increases in the range to 60–75 GPa and is about 30 $(\Omega$ cm$)^{-1}$. In this region the semiconductor regime is true for shocked alane. The conductivity of alane achieves approximately 500 $(\Omega$ cm$)^{-1}$ at 80–90 GPa. The conditions at which the transition from dielectric to conductive state are observed can be interpreted in frames of the conception of the dielectric catastrophe taking into consideration the significant difference between electronic states of isolated AlH$_3$ molecule and condensed alane.

*molodets@icp.ac.ru

[1] N. W. Ashcroft, Phys. Rev. Lett. **92**, 187002 (2004).

[2] C. J. Pickard and R. J. Needs, Phys. Rev. B **76**, 144114 (2007).

[3] I. Goncharenko, M. I. Eremets, M. Hanfland, J. S. Tse, M. Amboage, Y. Yao, and I. A. Trojan, Phys. Rev. Lett. **100**, 045504 (2008).

[4] A. I. Kolesnikov, V. E. Antonov, Yu. E. Markushkin, I. Natkaniec, and M. K. Sakharov, Phys. Rev. B **76**, 064302 (2007).

[5] F. M. Brower, N. E. Matzek, P. F. Reigler, H. W. Rinn, C. B. Roberts, D. L. Schmidt, J. A. Snover, and K. Terada, J. Am. Chem. Soc. **98**, 2450 (1976).

[6] V. E. Antonov, A. I. Kolesnikov, Yu. E. Markushkin, A. V. Palnichenko, Y. Ren, and M. K. Sakharov, J. Phys.: Condens. Matter **20**, 275204 (2008).

[7] G. I. Kanel, A. M. Molodets, and A. A. Vorobev, Combust., Explos. Shock Waves **10**, 793 (1974).

[8] V. V. Yakushev, Combust., Explos. Shock Waves **14**, 131 (1978).

[9] V. E. Fortov, V. V. Kim, I. V. Lomonosov, A. V. Matveichev, and A. V. Ostrik, Int. J. Impact Eng. **33**, 244 (2006).

[10] A. M. Molodets, D. V. Shakhray, A. A. Golyshev, L. V. Babare, and V. V. Avdonin, High Press. Res. **26**, 223 (2006).

[11] D. V. Shakhray, Ph. D. thesis, Institute of Problem of Chemical Physics, RAS, 2007.

[12] A. M. Molodets, High Press. Res. **25**, 267 (2005).

[13] A. Dewaele, P. Loubeyre, and M. Mezouar, Phys. Rev. B **70**, 094112 (2004).

[14] M. K. Sakharov, Ph. D. thesis, Institute of Solid State Physics, RAS, 2008.

[15] W. J. Nellis, S. T. Weir, and A. C. Mitchell, Phys. Rev. B **59**, 3434 (1999).

[16] K. F. Herzfeld, Phys. Rev. **29**, 701 (1927).

[17] D. A. Goldhammer, *Dispersion und Absorption des Lichtes in Ruhenden Isotropen Koerpern: Theorie und ihre Folerungen* (Teubner, Leipzig, Berlin, 1913).

[18] V. E. Fortov, I. T. Iakubov, and A. G. Khrapak, *Physics of Strongly Coupled Plasma* (Oxford University Press, Oxford, 2006).

[19] A. G. Khrapak and V. E. Fortov, JETP **106**, 910 (2008).

[20] T. A. Grzybowski and A. L. Ruoff, Phys. Rev. Lett. **53**, 489 (1984).

[21] T. Sako and G. H. F. Diercksen, J. Phys. B **36**, 3743 (2003).

[22] R. D. Shannon, J. Appl. Phys. **73**, 348 (1993).

[23] M. J. van Setten, V. A. Popa, G. A. de Wijs, and G. Brocks, Phys. Rev. B **75**, 035204 (2007).

[24] P. Vajeeston, P. Ravindran, B. C. Hauback, H. Fjellvag, A. Kjekshus, S. Furuseth, and M. Hanfland, Phys. Rev. B **73**, 224102 (2006).